



Published in final edited form as:

Structure. 2017 March 07; 25(3): 482–495. doi:10.1016/j.str.2017.01.014.

A partial calcium-free linker confers flexibility to inner-ear protocadherin-15

Robert E. Powers^{a,b}, Rachele Gaudet^{a,1}, and Marcos Sotomayor^{c,1,2}

^aDepartment of Molecular and Cellular Biology, Harvard University, Cambridge MA 02138, United States

^bBiophysics Graduate Program, Harvard University, Boston MA 02115, United States

^cDepartment of Chemistry and Biochemistry, The Ohio State University, Columbus OH 43210, United States

Summary

Tip links of the inner ear are protein filaments essential for hearing and balance. Two atypical cadherins, cadherin-23 and protocadherin-15, interact in a Ca^{2+} -dependent manner to form tip links. The largely unknown structure and mechanics of these proteins are integral to understanding how tip links pull on ion channels to initiate sensory perception. Protocadherin-15 has 11 extracellular cadherin (EC) repeats. Its EC3-4 linker lacks several of the canonical Ca^{2+} -binding residues, and contains an aspartate-to-alanine polymorphism (D414A) under positive selection in East Asian populations. We present structures of protocadherin-15 EC3-5 featuring two calcium-binding linker regions: canonical EC4-5 linker binding three calciums, and non-canonical EC3-4 linker binding only two calciums. Our structures and biochemical assays reveal little difference between the D414 and D414A variants. Simulations predict that the partial Ca^{2+} -free EC3-4 linker exhibits increased flexural flexibility without compromised mechanical strength, providing insight into the dynamics of tip links and other atypical cadherins.

Graphical abstract

¹Corresponding authors: Rachele Gaudet, Department of Molecular and Cellular Biology, Harvard University, 52 Oxford St, Cambridge, MA, 02138, USA, (617) 496-5616, gaudet@mcb.harvard.edu, ORCID: 0000-0002-9177-054X; Marcos Sotomayor, Department of Chemistry and Biochemistry, The Ohio State University, 484 W. 12th Avenue, Columbus OH 43210, USA, (614) 688-2070, sotomayor.8@osu.edu, ORCID: 0000-0002-3333-1805.

²Lead Contact

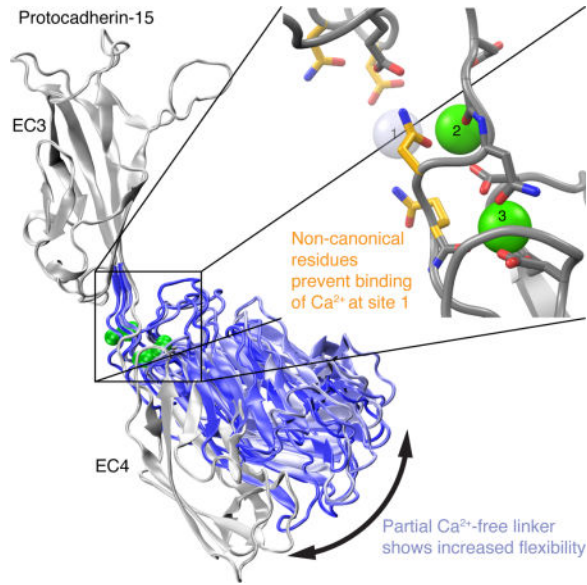
Publisher's Disclaimer: This is a PDF file of an unedited manuscript that has been accepted for publication. As a service to our customers we are providing this early version of the manuscript. The manuscript will undergo copyediting, typesetting, and review of the resulting proof before it is published in its final citable form. Please note that during the production process errors may be discovered which could affect the content, and all legal disclaimers that apply to the journal pertain.

Accession Numbers

The accession number for the PCDH15 EC3-5 and PCDH15 EC3-5 D414A structures reported here are PDB: 5T4M and 5T4N, respectively. The unprocessed diffraction images used to determine these structures were deposited in the SBGrid Data Bank with accession numbers 361, 362, and 363.

Author Contributions

M.S. determined the EC4-5 structure; R.E.P. conducted all other experiments. R.E.P. and M.S. ran the simulations. R.E.P., R.G., and M.S. designed the experiments, analyzed data and wrote the paper.



Keywords

Cadherin superfamily; tip link; mechanotransduction; X-ray crystallography; molecular dynamics simulation; hearing; deafness

Introduction

The vertebrate senses of hearing and balance rely on inner-ear hair cells to transform mechanical stimuli from sound and head movements into electric signals decoded by the brain. This mechanotransduction process occurs at the apical end of hair cells, where rows of stereocilia are arranged in order of increasing height to form sensory hair-cell bundles (Gillespie and Muller, 2009). The tip of each stereocilium is connected to its tallest neighbor by a fine “tip link” filament (Assad et al., 1991; Kachar et al., 2000; Pickles et al., 1984). As the bundle is deflected, tip links come under tension, pulling open mechanosensitive ion channels located at their lower end, depolarizing the hair cell to trigger sensory perception (Assad et al., 1991; Basu et al., 2016; Beurg et al., 2009).

The tip link is composed of the non-classical cadherin molecules cadherin-23 (CDH23) and protocadherin-15 (PCDH15) (Ahmed et al., 2006; Kazmierczak et al., 2007; Siemens et al., 2004; Söllner et al., 2004). Like the classical cadherins that mediate Ca^{2+} -dependent cell adhesion (Brasch et al., 2012; Hirano and Takeichi, 2012), CDH23 and PCDH15 have N-terminal extracellular cadherin (EC) repeats, followed by a transmembrane and a cytoplasmic domain that may interact with the cytoskeleton and other components of the transduction machinery (Beurg et al., 2015; Maeda et al., 2014; Pepermans and Petit, 2015). The EC repeats are similar, but not identical, in sequence, and are arranged in series with linker regions that bind Ca^{2+} ions. Unlike classical cadherins that typically have five EC repeats, CDH23 and PCDH15 are considerably longer and have 27 and 11 EC repeats respectively. The mature tip link is made of CDH23 and PCDH15 homodimers interacting at their N-terminal tips through a unique “handshake” interface distinct from that of classical

cadherins (Geng et al., 2013; Indzhukulian et al., 2013; Kazmierczak et al., 2007; Sotomayor et al., 2012).

PCDH15 also differs from classical cadherins in that several of its EC linkers lack typically conserved residues critical for Ca^{2+} binding (Figure 1A). Ca^{2+} is crucial to cadherin function, as bound ions rigidify linker regions allowing cadherins to assume an elongated, rod-like conformation that enables *trans* dimerization across adjacent cells. In the absence of Ca^{2+} , cadherin linkers become flexible, allowing adjacent EC repeats to move relative to one another (Cailliez and Lavery, 2005; Haussinger et al., 2002; Pokutta et al., 1994; Sotomayor and Schulten, 2008). In addition, cadherin mechanical strength is significantly reduced in the absence of Ca^{2+} (Oroz et al., 2011; Sotomayor and Schulten, 2008; Sotomayor et al., 2005). Tip links are also Ca^{2+} -sensitive, as removal of extracellular Ca^{2+} eliminates them and abolishes transduction currents in hair cells (Assad et al., 1991; Vollrath et al., 2007; Zhao et al., 1996). Given the importance of Ca^{2+} in cadherin function and mechanics, the absence of key Ca^{2+} -binding residues in certain atypical EC linkers of PCDH15 is intriguing.

PCDH15 also features a polymorphism under positive selection in East Asian populations: substitution of a negatively-charged aspartate residue (D414; processed protein numbering, corresponding to D435 in the unprocessed protein) for alanine is suggested to confer an evolutionary advantage through an unknown mechanism (Grossman et al., 2010, 2013). Yet D414 was hypothesized to coordinate Ca^{2+} (Grossman et al., 2010), suggesting the D414A polymorphism may impair Ca^{2+} binding and paradoxically compromise mechanical strength. Interestingly, this polymorphism is located at an atypical linker region between repeats EC3 and EC4 of PCDH15, where several residue positions typically involved in Ca^{2+} binding have non-canonical substitutions (Figure 1A), as observed for some members of the cadherin superfamily (Harrison et al., 2016; Jin et al., 2012; Tariq et al., 2015; Tsukasaki et al., 2014).

To elucidate the biophysical properties of atypical cadherin linker regions and the effect of the D414A polymorphism, we determined the X-ray crystal structure of PCDH15 EC3-5. The linker between repeats EC3 and EC4 was captured in two bent conformations and features only two bound Ca^{2+} ions, as opposed to the canonical linker with three bound Ca^{2+} ions observed in EC4-5 and in all non-desmosomal classical cadherins of known structure. In addition, the D414A polymorphism does not alter PCDH15's structure significantly. Finally, our structures and molecular dynamics simulations predict that atypical, partial Ca^{2+} -free EC linkers retain considerable mechanical strength but display increased flexibility that might be functionally relevant.

Results

The PCDH15 EC3-5 repeats form mostly canonical cadherin repeat structures

Classical cadherins feature conserved Ca^{2+} -binding motifs that coordinate three Ca^{2+} ions at the linker between two sequential EC repeats (Figure 1A,D). A DXE motif and conserved glutamate (XEX) in the pre-linker repeat coordinate Ca^{2+} ions at sites 1 and 2, while a DXD and conserved aspartate (XDX) in the post-linker EC repeat coordinate Ca^{2+} ions at sites 2 and 3. Finally, the linker loop connecting two EC repeats includes the classical cadherin

DXNDN motif, which contributes to the coordination of all three Ca^{2+} ions (Boggon et al., 2002; Nagar et al., 1996). Sequence alignment of the 11 PCDH15 EC repeats reveals that many linkers have non-canonical substitutions within these motifs (Figure 1A). In particular, EC3 displays six such substitutions, half of which occur at positions coordinating the site 1 and site 2 Ca^{2+} ions in the EC3-4 linker. These substitutions are conserved across species (Figure 1B), suggesting a functional importance, although such substitutions could compromise the ability of the EC3-4 linker to bind Ca^{2+} , which is essential for tip link integrity (Assad et al., 1991; Vollrath et al., 2007).

To investigate the impact of the non-canonical substitutions on the EC3-4 linker, we determined the structure of a PCDH15 fragment containing EC3 through EC5 (EC3-5) using X-ray crystallography (Table 1). The asymmetric unit contains two EC3-5 molecules (chains A and B), which are similar in structure except for a rigid-body motion described below. Each EC repeat exhibits the same Greek-key fold observed for classical cadherins, comprising seven β -strands (labeled A to G) in two β -sheets (Figure 1C) (Boggon et al., 2002; Nagar et al., 1996). However, EC3 and EC4 feature conserved loops that are absent from classical EC repeats (Figure 1A–C). Unique to EC3, an N-terminal cysteine-stapled loop interrupts strand A, extending outward as a β -hairpin clamped by a disulfide bond between residues C247 and C256. Both EC3 and EC4 have insertions before or within strand B, which in EC4 forms an extended loop interrupting strand B (Figure 1C). The function of these conserved loop insertions is unknown; one possibility is that they participate in PCDH15 dimerization in tip links, which are believed to be $(\text{CDH23})_2(\text{PCDH15})_2$ assemblies (Kazmierczak et al., 2007). Other than these loops, the individual repeats in the EC3-5 fragment adhere to classical EC structure.

The partial Ca^{2+} -free EC3-4 linker only binds two Ca^{2+} ions

Strikingly, while the EC4-5 linker has three Ca^{2+} ions, consistent with its canonical Ca^{2+} -coordinating sequence motifs (Figure 1D), we only observed two Ca^{2+} ions, at sites 2 and 3, in the EC3-4 linker. This was consistent in both copies of EC3-5 in the asymmetric unit (Figure 1E–F). No unassigned electron density was observed at the potential Ca^{2+} -binding site 1 (Figure 2), despite the high Ca^{2+} concentration (150 mM) present during crystallization. Most available cadherin structures contain linkers that bind three Ca^{2+} ions. However, a *Drosophila* N-cadherin linker binds no Ca^{2+} ions at all (Jin et al., 2012), and Desmoglein-2 and -3 structures show a partial Ca^{2+} -free linker between ECs 3 and 4 with Ca^{2+} ions at sites 1 and 2, but none at site 3 (Harrison et al., 2016). Thus, the PCDH15 EC3-4 linker is the first observed partial Ca^{2+} -free linker with Ca^{2+} at sites 2 and 3 only. Comparison of PCDH15 EC3-4 with Desmoglein-2 EC3-4 shows a displacement of the repeat closest to the missing Ca^{2+} (Figure 3), suggesting that distinct Ca^{2+} -binding patterns increase the conformational diversity of cadherins.

The non-canonical substitutions in the EC3-4 linker Ca^{2+} -binding motifs have clear structural consequences, as can be inferred from comparing the EC3-4 and EC4-5 linkers (Figure 1D–F). First, Ca^{2+} coordination at site 3 is similar to that observed in the canonical EC4-5 linker, except that a water molecule replaces a carbonyl ligand from the bottom repeat's B-C loop (Figure 1D–F)—interestingly, this loop also features the D414A

polymorphism. Second, Ca^{2+} coordination at the EC3-4 linker site 2 is incomplete due to substitutions in the DXNDN and DXE motifs: whereas the EC4-5 site 2 Ca^{2+} has six ligands, the EC3-4 site 2 Ca^{2+} has three and five protein-based ligands in chains A and B of the asymmetric unit, respectively. In EC4-5, the 480-DANDN-484 motif provides three ligands (D480, carbonyl of A481, and D483). In EC3-4, the 366-DENNQ-370 motif similarly provides Ca^{2+} ligands from the carbonyl of E367, and N369. D366 provides two ligands in chain B whereas it is too far to directly participate in the binding site in chain A, because of the different EC3-EC4 inter-repeat orientations detailed below. Similarly, while in EC4-5 the canonical DXE glutamate E451 coordinates both Ca^{2+} ions 1 and 2, the corresponding EC3-4 linker NRD motif aspartate D335 is shorter and does not reach site 2. Finally, while the EC3-4 site 1 retains some Ca^{2+} -coordinating groups, the DXNDN-to-DENNQ and DRE-to-NRD substitutions eliminate three of the four to five ligands seen in canonical linker structures, thus explaining the lack of Ca^{2+} binding at site 1.

The partial Ca^{2+} -free EC3-4 linker is more flexible than canonical linkers

A comparison of the two chains observed in the asymmetric unit provides clues as to the consequences of a partial Ca^{2+} -free EC3-4 linker. In repeat-by-repeat comparison, the root mean square deviations (RMSD) for Ca positions are 0.91, 0.14, and 0.29 Å for EC3, EC4 and EC5, respectively. However, aligning just the EC4-5 repeats of the two monomers (RMSD = 0.25 Å) reveals a pronounced difference in the inter-repeat tilt angle between EC3 and EC4, 134° vs. 112° (chain A vs. chain B; Figure 4A). In addition to the difference between the two monomers, these tilt angles are smaller than the EC4-EC5 angle of 162°, which is comparable to that of canonical cadherin linker structures (Nicoludis et al., 2015). In the canonical EC4-5 linker, EC4 is effectively clamped to EC5 by the coordination of the site 1 and 2 Ca^{2+} ions by D449, E451, and E385. In contrast, the apparent EC3-4 linker flexibility is consistent with the absence of Ca^{2+} at site 1 and lack of coordination of Ca^{2+} ion 2 by D335 or E267. As a result, there are no interactions between the core β strands (A, B, and F) of EC3 and the bound Ca^{2+} ions at EC4, allowing EC3 to rotate relative to EC4.

To further investigate the extent of inter-repeat flexibility, we performed 100-ns long equilibrium molecular dynamics (MD) simulations for the EC3-4 repeats of each chain (Table S1; simulations S-3 and S-4 for chains A and B, respectively). For comparison, we simulated EC4-5 (simulation S-1) as a representative canonical linker, and also EC3-4 with all Ca^{2+} ions removed *in silico* (apo-EC3-4; S-2). For each simulation we quantified dynamics by calculating both the tilt (θ) and azimuthal (φ) angles between the principal axes of the consecutive repeats (Figure 4B). As observed in simulations of other cadherin linkers (Cailliez and Lavery, 2005; Manibog et al., 2014; Sotomayor and Schulten, 2008; Sotomayor et al., 2010), the canonical EC4-5 linker was nearly straight and quite rigid over the entire simulation (Figure 4C,D). Conversely, apo-EC3-4 was highly flexible, exploring a large range of tilt and azimuthal angles (Figure 4C,D). These results are consistent with *in vitro* and *in silico* studies that indicate that cadherins, including CDH23, are rigid rods in the presence of Ca^{2+} , but highly flexible in its absence (Cailliez and Lavery, 2005; Haussinger et al., 2002; Kazmierczak et al., 2007; Manibog et al., 2014; Pokutta et al., 1994; Sotomayor and Schulten, 2008; Sotomayor et al., 2010).

In both partial Ca^{2+} -free EC3-4 simulations the linker displayed a larger bend, with an average θ of $106 \pm 16^\circ$ and $79 \pm 10^\circ$ for chains A (S-3) and B (S-4) respectively, compared to the canonical EC4-5 linker ($\theta = 166 \pm 4^\circ$) (Figures 4C,D, S1, and S2). The EC3-4 linker also showed more flexibility, as indicated by the larger standard deviations. This is consistent with the lack of interaction between the EC3 core and the Ca^{2+} ions, which would serve to link the cores of EC3 and EC4. However, the partial Ca^{2+} -free EC3-4 was still more rigid than apo-EC3-4 ($\theta = 89 \pm 43^\circ$; Figures 4C,D, S1, and S2) revealing that the two bound Ca^{2+} ions do exert a rigidifying effect. Consistent with the increased flexibility, we did not observe any non-canonical polar or hydrophobic contacts that could provide alternative means of rigidifying the EC3-EC4 interface. As mentioned above, D366 displays two distinct conformations within the crystal structure (Figure 1E,F): in chain A D366 points away from the site 2 Ca^{2+} ion, while in chain B D366 coordinates this Ca^{2+} ion. Interestingly, D366 rapidly flips –within the first few nanoseconds of equilibrium simulations of chain A–and then stably coordinates the site 2 Ca^{2+} ion as it does in chain B (Figure S3), suggesting that this interaction is generally favored. Thus our structures and simulations indicate that Ca^{2+} stoichiometry modulates inter-repeat motion with partial Ca^{2+} -free linkers exhibiting an intermediate level of flexibility and bend.

Site 2 and 3 Ca^{2+} ions stabilize the EC3-4 linker under force

Given the role of PCDH15 in mechanotransduction, the protein must withstand forces ranging from 1 pN to greater than 100 pN as suggested by experimental measurements (Cheung and Corey, 2006; Howard and Hudspeth, 1988; Jaramillo and Hudspeth, 1993). Because Ca^{2+} is important for the mechanical strength of cadherins (Oroz et al., 2011; Sotomayor and Schulten, 2008; Sotomayor et al., 2005), we investigated how the partial Ca^{2+} -free EC3-4 linker impacts the strength of PCDH15 using steered molecular dynamics (SMD) simulations. In these simulations, we stretched EC3-5 by applying forces through springs attached to the N- and C-termini, which moved in opposite directions at constant speeds of 10, 1, and 0.1 nm/ns (Grubmuller, 2005; Isralewitz et al., 2001; Sotomayor and Schulten, 2007). These SMD simulations are summarized in Table S2.

In initial simulations in which the stretching forces were applied to single Ca atoms (Ca of P242 and P587), core β -sheets rapidly ruptured before any linker ruptured (Figure S4; simulations S-7b-d, S-8b-d, S-9b-d). This could be due to the non-physiological N- and C-termini of our PCDH15 fragment. In the tip link, forces applied to EC3 and EC5 would be distributed across various β strands linked to Ca^{2+} ions bound in adjacent linkers. To better mimic these physiological conditions, we performed SMD simulations in which force was applied to the center of mass of a group of Ca atoms distributed at the ends of EC3 and EC5 (Figure 5A; S-7e-g, S-8e-g, S-9e-g). In these simulations, rupturing events localized to linkers even at the fastest pulling speed (10 nm/ns).

At 1 and 0.1 nm/ns pulling speeds (simulations S-7f,g), the EC3-4 linker ruptured first, as non-covalent interactions between the site 2 Ca^{2+} and D411 as well as the site 3 Ca^{2+} and N368 were broken, resulting in rapid extension of the linker strand and a drop in applied force (Figures 5B,C,E,G and S5B,C). Following linker extension, a second rupture occurred when the interaction of Q370 and site 3 Ca^{2+} broke and F374 was pulled out of the EC4

hydrophobic core (Figures 5D,E,G and S5B,C). Eventually, at the maximum and final force peak, strand A' was extracted from EC4 (Figures 5G and S5B–E). The unfolding pathway was only slightly different at a faster pulling speed of 10 nm/ns (simulation S-7e; Figures S5B,F,G).

While the partial Ca²⁺-free EC3-4 linker was the site of various ruptures, the EC4-5 linker, with three Ca²⁺ ions, remained intact (Figures 5G and S5B,C), indicating that the lack of a site 1 Ca²⁺ and non-canonical coordination of the site 2 Ca²⁺ decreased the EC3-4 linker strength. To ascertain whether the two Ca²⁺ ions in the EC3-4 linker contributed to stability, we performed SMD simulations where these two Ca²⁺ ions were removed *in silico* (simulations S-8e–g). At all pulling speeds, the apo-EC3-4 linker stretched more progressively with time, compared to a stepwise manner when Ca²⁺ was present (Figures 5G,H, S5B,C and S6B,C). As in the Ca²⁺-bound simulations, a force peak was associated with F374 extraction from the EC4 hydrophobic core (Figures 5F,H and S6B–E). However, this occurred at a lower force when Ca²⁺ was absent: 753 vs 921 pN at a 0.1 nm/ns pulling speed (S-7g, S-8g), and 728 vs 1106 pN at a 1 nm/ns (S-7f, S-8f), for apo and Ca²⁺-bound EC3-4 linker respectively (Figure 5E,F). Overall these simulations indicate that, despite missing a site 1 Ca²⁺, the partial EC3-4 linker is still stabilized by the remaining site 2 and site 3 Ca²⁺ ions.

Ex-vivo measurements of receptor potentials or currents during deflection of hair cell bundles by a flexible probe or laser-trapped beads, respectively, suggest that hair-cell channels are connected to a soft spring that modulates their gating. This “gating spring” has a stiffness of ~ 1 mN/m (Cheung and Corey, 2006; Howard and Hudspeth, 1988). Although the tip link has been proposed to be the gating spring, *in situ* ultrastructural studies suggest that tip links could be stiff (Kachar et al., 2000). Previous SMD simulations of both CDH23 and PCDH15 fragments that contain canonical calcium linkers also predicted that tip link proteins are two orders of magnitude stiffer than the gating spring (Sotomayor et al., 2010, 2012). To evaluate whether non-canonical linkers could provide some elasticity to the tip link, we estimated the partial Ca²⁺-free linker stiffness as the slope of the force versus end-to-end distance curve prior to the first rupture and force peak (Figure 5E,F). At the slowest pulling speed (S-7g), the EC3-5 stiffness was 627 mN/m. In the absence of calcium at EC3-4, two distinct extension regimes were observed prior to the first force peak (Figure 5F; S-8g). The first regime, corresponding to EC3-4 linker extension, displayed a stiffness of 8 mN/m. Thus if EC3-4 sites are not occupied by Ca²⁺, this linker may contribute some elasticity to the gating spring, with a limited extension range of ~1 nm. In the second regime the stiffness was 659 mN/m, similar to the EC3-5 stiffness. A ~600 mN/m stiffness for three EC repeats extrapolated to the entire tip link (two parallel sets of 38 repeats in a heterotetrameric tip link) would be ~90 mN/m, too stiff to account for the gating spring elasticity unless the stiffness decreases significantly at slower pulling speeds or other EC repeats are somehow softer.

The D414A polymorphism does not affect PCDH15 EC3-5 structure or dynamics

The D414A polymorphism, under positive selection in East Asian populations (Grossman et al., 2010, 2013), is within the EC3-4 linker, where a previous homology model implicated

this residue in binding the site 3 Ca^{2+} ion. Our EC3-5 structure revealed that although residue D414 does not directly coordinate Ca^{2+} in the EC3-4 linker, it is in the B-C loop near the site 3 Ca^{2+} ion (Figure 1). In canonical linkers this loop participates in Ca^{2+} ion 3 coordination through a backbone carbonyl (Boggon et al., 2002). In PCDH15 EC3-4, the B-C loop extends away from Ca^{2+} ion 3, preventing such coordination. To determine whether the D414A polymorphism causes a structural change within this loop or any other part of EC3-5, we determined the structure of EC3-5^{D414A}, which crystallized in the same space group as EC3-5 under nearly identical conditions (Table 1). The EC3-5^{D414A} structure revealed no large structural changes as compared to EC3-5 (RMSD = 0.30 and 0.25 Å, for chains A and B, respectively). The EC4 B-C loop adopted nearly the same extended conformation as in EC3-5^{D414}, except that the A414 backbone was best modeled in an α -helical conformation, while the D414 backbone best fit a β -sheet conformation (Figure 6A,B). However, electron density for the B-C loop is weaker than in most of the protein in both structures, making this assignment tentative and suggesting this loop is somewhat flexible in both cases.

To further investigate any potential impact of the D414A polymorphism, we tested whether it alters inter-repeat motion by performing equilibrium simulations of both EC3-4^{D414A} chains (simulations S-5 and S-6). EC3-4^{D414A} behaved very similarly to EC3-4 (Figures 4C,D, 6C-F, S1, and S2). Furthermore, SMD simulations of EC3-5^{D414A} (S-9) were similar to those of EC3-5 (S-7). An initial force peak and a rapid extension of the EC3-4 linker (Figures 6G,H and S7B-D) was followed by extraction of F374 from the EC4 hydrophobic core at forces (1237 pN at 1 nm/ns and 792 pN at 0.1 nm/ns, simulations S-9f-g) comparable to that of EC3-5 (Figures 5E and 6G,H; Figure S7B,E). At the slowest pulling speed (simulation S-9g), EC3-5^{D414A} displayed a stiffness of 741 mN/m prior to the first force peak, similar to EC3-5 (Figures 5E and 6G). Thus, our simulations predict that the D414A polymorphism does not significantly alter the mechanical properties of the EC3-5^{D414A} fragment.

Finally, we used a competition assay with a fluorescent Ca^{2+} indicator (Sotomayor et al., 2010) to determine whether the D414A polymorphism changes the Ca^{2+} -binding affinity of EC3-4. At Ca^{2+} concentrations ranging from 0 to 215 μM , the Ca^{2+} -binding behavior of EC3-4 and EC3-4^{D414A} were essentially indistinguishable (Figure 6I), indicating that the D414A polymorphism has no appreciable impact on the Ca^{2+} -binding affinity of the EC3-4 linker. The fluorescence data was fit using a two-binding site model (Andre and Linse, 2002) to obtain approximate K_d values for the site 2 and 3 Ca^{2+} ions. The resulting K_d values are 45 (\pm 26) and >100 μM for EC3-4 and 101 (\pm 57) and >100 μM μM for EC3-4^{D414A} ($n = 4$ for each construct). The EC3-4 Ca^{2+} -binding sites therefore exhibit lower Ca^{2+} -affinity than canonical linkers (Courjean et al., 2008; Pokutta et al., 1994; Sotomayor et al., 2010), consistent with the reduced number of ligands in both EC3-4 linker sites 2 and 3.

Discussion

In this study we present the first high-resolution structure of PCDH15 EC3-5, which features a novel, partial Ca^{2+} -free cadherin linker between EC3 and EC4 that binds only two Ca^{2+} ions at sites 2 and 3. This particular Ca^{2+} stoichiometry is a consequence of non-canonical

substitutions within canonical cadherin Ca^{2+} -binding motifs. These substitutions remove a number of important Ca^{2+} ligands, completely disrupting site 1 Ca^{2+} binding and reducing binding affinity at sites 2 and 3. Two distinct conformations of the EC3-4 repeats observed in our crystal structure strongly suggest enhanced flexibility at this linker. Our extensive simulations of EC3-4 also support that such partial Ca^{2+} -free linker is more flexible and bent than canonical linkers that bind three Ca^{2+} ions, but still more rigid and mechanically stronger than linkers completely void of Ca^{2+} . Thus, our results indicate that the Ca^{2+} -binding stoichiometry of cadherin linker regions modulates inter-repeat flexibility and shape.

The absence of Ca^{2+} at site 1 in the PCDH15 EC3-4 linker allows for more conformational freedom, but the Ca^{2+} ions bound at sites 2 and 3 ensure that this does not come at a cost of significantly impaired mechanical strength. Our SMD simulations revealed that the partial Ca^{2+} -free linker withstands forces nearly as large as those withstood by canonical linkers. Maintaining this strength is important given the role of PCDH15 in transmitting sound- and head movement-induced forces within the context of the tip link.

The increased flexibility of the EC3-4 linker is surprising given that certain deafness-causing mutations within CDH23 linkers increase inter-repeat motion and decrease affinity for Ca^{2+} (Sotomayor et al., 2010). However, conservation across species of the non-canonical substitutions within the EC3-4 linker indicates a functional importance for this flexibility. Furthermore, using our structure and its non-canonical sites as a guide, we predict that the EC2-3 and EC5-6 linkers in PCDH15 bind fewer than three Ca^{2+} ions while the EC9-10 linker, with no intact Ca^{2+} -binding motif, should be entirely Ca^{2+} -free. CDH23 also contains 4 linkers (EC12-13, EC21-22, EC24-25, EC25-26) that have at least one atypical amino acid in their Ca^{2+} -binding motifs that could prevent these linkers from binding Ca^{2+} at particular sites. Thus, potentially flexible linkers located at particular points along PCDH15 and CDH23 may fine-tune the mechanical stiffness of the two molecules, thereby optimizing tip-link assembly and transduction of physiological mechanical forces. Further experiments will be needed to explore the functional consequence of this increased flexibility at EC3-4 and the other non-canonical PCDH15 linkers within the context of the entire tip link and larger mechanotransduction machinery of the hair cell. In particular, non-canonical linkers within PCDH15 may play a role in the formation and function of the tip link PCDH15 parallel homodimer (Kazmierczak et al., 2007), which in turn may have a different elastic response than the individual components.

The role played by non-canonical PCDH15 linkers must also be considered in the physiological context of hair cells. The partial Ca^{2+} -free EC3-4 linker with reduced binding affinity for Ca^{2+} might not be fully occupied in the environment that surrounds it. The endolymph that bathes hair cells is characterized by low Ca^{2+} concentrations that range from 20 to 40 μM in the cochlea, and $>100 \mu\text{M}$ in the vestibular system (Bosher and Warren, 1978; Nakaya et al., 2007; Salt et al., 1989). Thus, our data suggest that models of tip link function must incorporate the thermodynamics of Ca^{2+} binding to non-canonical, partial Ca^{2+} -free linkers.

Despite exploring calcium binding, protein structure, conformational flexibility and mechanical strength, we observed no clear structural or biochemical alterations caused by

the D414A polymorphism. Thus the evolutionary advantage suggested by its positive selection in the East Asian population (Grossman et al., 2010, 2013) may be conferred through other mechanisms not tested here. Of note, the corresponding nucleotide polymorphism is immediately 5' to a splice donor site in the mRNA, which is used with two alternative splice acceptor sites (Ahmed et al., 2006). While we focused on the isoform most commonly observed in available mouse and human mRNA sequences, alternatively spliced isoforms contain seven additional residues (VPPSGVP; corresponding to exon 12a) immediately following D414 in the loop between the B and C strands of EC4. Thus the polymorphism may modify mRNA processing efficiency and/or the ratio of isoforms, which could be investigated through transcriptomics analyses of tissue samples from individuals with and without the D414A polymorphism. Alternatively, the D414A polymorphism may have more marked biochemical consequences on the alternate protein isoforms. Other possible mechanisms include changes in protein folding efficiency, trafficking or tip link assembly. The D414A polymorphism was also associated with deafness in a genetic study of a consanguineous Pakistani family (Saleha et al., 2016), which is surprising since it is very common—homozygous in 1050 of 8255 available South Asian exomes and present at frequency of 0.24 over all available exomes (Lek et al., 2016). Our results suggest the D414A polymorphism is unlikely to cause a severe loss-of-function and deafness phenotype on its own.

More generally, the frequency of non-canonical linkers within the larger cadherin family has recently become evident. *Drosophila* N-cadherin's Ca²⁺-free linker enables a 'jack-knife' conformation that may facilitate a unique binding mode reminiscent of Dscam molecules (Jin et al., 2012; Sawaya et al., 2008). Non-canonical cadherin linkers also facilitate the bending of the giant cadherins Fat and Dachshous, allowing them to fit into confined intercellular junctions (Tsukasaki et al., 2014). Most recently, crystal structures of desmoglein 2 and 3 (Harrison et al., 2016) revealed partial-Ca²⁺ free linkers that only bind Ca²⁺ at sites 1 and 2 due to substitutions at certain site 3 Ca²⁺-binding residues—namely the middle asparagine in the DXNDN motif (Figure 3). These partial-Ca²⁺ free desmoglein linkers, much like the PCDH15 EC3-4 linker, create a pronounced bend between repeats (Figure 3B), and it is hypothesized that this flexing within desmosomal cadherins may account for the plasticity of desmosomes (Harrison et al., 2016; Tariq et al., 2015). Our structure represents the first example of a non-canonical partial Ca²⁺-free linker with Ca²⁺ ions at positions 2 and 3, and our analysis of PCDH15 sequences, in conjunction with other extensive analyses of the cadherin superfamily (Jin et al., 2012), suggest that there are additional examples. Our insights into the structure and dynamics of partial-Ca²⁺ free linkers will therefore aid in future explorations of these unique cadherins that perform many functions underlying multicellular life.

Experimental Procedures

Cloning, expression, and purification of PCDH15 fragments

Fragments of *H. sapiens* protocadherin-15 (NM_001142771.1) containing EC3-4 (residues P242-N484; numbering corresponding to processed protein) and EC3-5 (residues P242-F595) were cloned into the pET21a NheI and XhoI sites (Novagen). *M. musculus*

protocadherin-15 (NM_001142746.1) EC4-5 (MmEC4-5; residues T375 to F595 in processed protein) was cloned into the pET21a NdeI and XhoI sites (Novagen). D414A was generated using QuikChange (Stratagene). Constructs were expressed in *E. coli* BL21-Gold(DE3) (Stratagene) in lysogeny broth (LB) induced at OD₆₀₀ ~ 0.6–1.0 with 800 μM IPTG at 37 °C for 18 hr. Cells were lysed by sonication in denaturing buffer (20 mM HEPES pH 7.5, 10 mM CaCl₂, 6 M guanidinium chloride, 20 mM imidazole pH 7.5). Cleared lysates were loaded onto Ni-sepharose (GE Healthcare), eluted with denaturing buffer supplemented with 500 mM imidazole pH 7.5, and refolded by dialysis against 20 mM Tris HCl pH 8.0, 10 mM CaCl₂, and 400 mM L-arginine hydrochloride (and 2 mM DTT for MmEC4-5) overnight at 4 °C using a 2000 molecular weight cut-off (MWCO) membrane. Refolded protein was further purified by size-exclusion chromatography on a Superdex200 column (GE Healthcare) and concentrated by ultrafiltration on a 10,000 MWCO filter (Amicon Ultra, EMD Millipore).

Crystallization, data collection, and structure determination

MmEC4-5 crystals were obtained in 0.1 M Bicine pH 9.0, 0.5 M CaCl₂. EC3-5 crystals were grown at 4 °C by hanging drop vapor diffusion, mixing protein (7–8 mg/ml) 1:1 with reservoir (0.1 M sodium cacodylate pH 6.0, 150 mM CaCl₂ for EC3-5; 0.1 M sodium cacodylate pH 5.8, 150 mM CaCl₂ for EC3-5^{D414A}). Crystals were cryoprotected in reservoir supplemented with 20–25% glycerol and 4% PEG 8000 and cryo-cooled in liquid N₂. X-ray diffraction data were collected as indicated in Table 1 and processed with HKL2000 (Otwinowski and Minor, 1997). EC3-5 structures were determined by molecular replacement using a partially-refined structure of MmEC4-5 (Table 1; based on PDB code: 2O72) as search model with PHENIX (Adams et al., 2010). Model building was done using COOT (Emsley et al., 2010), PHENIX Autobuild, and PHENIX refine using NCS and TLS restraints. For EC3-5^{D414A}, reference model restraints using the EC3-5 structure were implemented. Both structures include residues 242–587 (chain A), and 242–595 (chain B) except for residues 288–299 (EC3-5 chain B), 287–297 (EC3-5^{D414A} chain A), and 288–299 (EC3-5^{D414A} chain B), which were not modeled due to poor electron density.

Simulated Systems

Simulation systems were built in VMD using the autopsfgen, solvate, autoionize, and orient plugins (Humphrey et al., 1996). Hydrogens were automatically added to protein structures and crystallographic waters. For fragments that contained omitted regions, corresponding residues from EC3-5 chain A were used as a model. Residues simulated were 242–482 for EC3-4, 369–587 for EC4-5, and 242–587 for EC3-5. The disulfide between C247 and C256 was explicitly modeled and residues D, E, K, and R were assumed to be charged. Histidines were assumed neutral and assigned protonation states that favored formation of evident hydrogen bonds. Systems were solvated by randomly placing additional waters and ions to a final concentration of 150 mM KCl.

Molecular Dynamics

Simulations were performed as previously described (Sotomayor et al., 2010) using NAMD 2.10b2 (Phillips et al., 2005), the CHARMM36 force field that includes the CMAP correction (Best et al., 2012), and the TIP3P water model (Jorgensen et al., 1983). Systems

were equilibrated with 1,000 steps of minimization followed by 0.1 ns of simulation where the backbone was restrained with $k = 1 \text{ kcal mol}^{-1} \text{ \AA}^{-2}$. For the remainder of the simulations, restraints of $k = 1 \text{ kcal mol}^{-1} \text{ \AA}^{-2}$ were placed on the Ca atoms of residues 283, 305, and 358 (EC3-4 simulations) or 405, 424, and 472 (EC4-5 simulations) to prevent interactions across the periodic boundary but still allow intradomain and inter-repeat flexing. An additional 1 ns was simulated in the NpT ensemble with the Langevin damping constant γ set to 1 ps^{-1} before setting it to 0.1 ps^{-1} for the rest of the simulation. Periodic boundary conditions were imposed, along with a 12-\AA cutoff for short-range interactions (switching function starting at 10 \AA), and a grid point density $>1 \text{ \AA}^{-3}$ for the calculation of long-range electrostatic force without cutoff using the Particle Mesh Ewald method. Simulations were performed using uniform 2-fs time steps, with SHAKE enabled. A constant temperature of 300 K was maintained through Langevin dynamics. To maintain a constant pressure for the NpT ensemble, the hybrid Nosé-Hover Langevin piston method was used with a time decay period of 200 fs and damping time constant of 50 fs. Coordinates were recorded every 1 ps. Constant velocity stretching simulations (Israelewitz et al., 2001; Sotomayor and Schulten, 2007) were carried out using the same parameters mentioned above with Ca atoms of N- and C-terminal residues (or the center of mass of groups Ca atoms) attached to separate virtual springs ($k = 1 \text{ kcal mol}^{-1} \text{ \AA}^{-2}$). The free ends of the springs were moved away from each other at constant velocity along the x -axis.

Simulations and analysis tools

RMSD values were calculated in PyMOL (Schrödinger, LLC) using the align command. Tilt angles were computed as the complement of the dot product of the third principal axes of adjacent repeats. For azimuthal angles, the first repeat's third principal axis was aligned to the z -axis, then the projection of the adjacent repeat's third principal axis onto the x - y plane was calculated and plotted, and the azimuthal angle calculated using this projected point. Principal axes were computed using the VMD Orient plugin. Forces applied in SMD simulations were computed using the extension of the virtual springs. Plotted forces correspond to those applied to N-terminal atoms. Maximum force peaks were computed from the mean of N- and C-terminal peaks obtained from 50-ps running averages. Sequence alignments were performed using MUSCLE (Edgar, 2004). Numerical analysis and plots were prepared using MATLAB R2014b (MathWorks). Molecular images were created with VMD (Humphrey et al., 1996) or PyMOL (Schrödinger, LLC).

Fluorescence competition assay

Competition assay was performed as previously described (Sotomayor et al., 2010). Briefly: assay buffer (100 mM KCl, 10 mM MOPS, pH 7.5) was incubated with Chelex-100 resin (BioRad) for two days prior to use. The EC3-4 and EC3-4^{D414A} fragments were stripped of bound Ca^{2+} following purification by three successive incubations with fresh Chelex-100 resin. Absorbance at 280 nm was used to determine protein concentration. Assays were performed at $25 \text{ }^\circ\text{C}$ in 2-mL cuvettes containing $2.5 \text{ }\mu\text{M}$ mag-fluo-4 (Invitrogen) and $150 \text{ }\mu\text{M}$ protein. CaCl_2 was titrated in stepwise and fluorescence was monitored using a fluorescence spectrometer (Fluorolog-3, Instruments S. A., Inc.). Excitation and emission wavelengths were set at 430 nm and 530 nm respectively. As a control, titration of mag-fluo-4 in the absence of protein yielded an apparent K_d of $30 \text{ }\mu\text{M}$, as previously reported

(Sotomayor et al., 2010). Fluorescence curves were then fit using the CaLigator software (Andre and Linse, 2002) assuming a binding stoichiometry of two Ca^{2+} ions per protein molecule. Experiments were conducted in duplicate and repeated twice, and reported values are averages of the K_d calculated in each individual case.

Supplementary Material

Refer to Web version on PubMed Central for supplementary material.

Acknowledgments

We thank members of the Gaudet, Leschziner, and D'Souza labs for technical suggestions and discussions. This work was supported by the National Institutes of Health (NIH; K99/R00 DC012534-01 to M.S. and R01 DC02281 to D.P. Corey and R.G.). All simulations were performed using the Oakley supercomputer at the Ohio Supercomputing Center (OSC-PAS1037). Use of Advanced Photon Source Northeastern Collaborative Access Team beamlines was supported by NIH P41 GM103403, NIH-ORIP HEI grant S10 RR029205, and Department of Energy contract DE-AC02-06CH11357.

References

- Adams PD, Afonine PV, Bunkóczi G, Chen VB, Davis IW, Echols N, Headd JJ, Hung L-W, Kapral GJ, Grosse-Kunstleve RW. PHENIX: a comprehensive Python-based system for macromolecular structure solution. *Acta Crystallogr Sect D Biol Crystallogr*. 2010; 66:213–221. [PubMed: 20124702]
- Ahmed ZM, Goodyear R, Riazuddin S, Lagziel A, Legan PK, Behra M, Burgess SM, Lilley KS, Wilcox ER, Riazuddin S, et al. The tip-link antigen, a protein associated with the transduction complex of sensory hair cells, is protocadherin-15. *J Neurosci*. 2006; 26:7022–7034. [PubMed: 16807332]
- Andre I, Linse S. Measurement of Ca^{2+} -binding constants of proteins and presentation of the CaLigator software. *Anal Biochem*. 2002; 305:195–205. [PubMed: 12054448]
- Assad JA, Shepherd GM, Corey DP. Tip-link integrity and mechanical transduction in vertebrate hair cells. *Neuron*. 1991; 7:985–994. [PubMed: 1764247]
- Basu A, Lagier S, Vologodskaya M, Fabella BA, Hudspeth AJ. Direct mechanical stimulation of tip links in hair cells through DNA tethers. *Elife*. 2016; 5
- Best RB, Zhu X, Shim J, Lopes PE, Mittal J, Feig M, Mackerell AD Jr. Optimization of the additive CHARMM all-atom protein force field targeting improved sampling of the backbone phi, psi and side-chain chi(1) and chi(2) dihedral angles. *J Chem Theory Comput*. 2012; 8:3257–3273. [PubMed: 23341755]
- Beurg M, Fettiplace R, Nam JH, Ricci AJ. Localization of inner hair cell mechanotransducer channels using high-speed calcium imaging. *Nat Neurosci*. 2009; 12:553–558. [PubMed: 19330002]
- Beurg M, Xiong W, Zhao B, Müller U, Fettiplace R. Subunit determination of the conductance of hair-cell mechanotransducer channels. *Proc Natl Acad Sci U S A*. 2015; 112:1589–1594. [PubMed: 25550511]
- Boggon TJ, Murray J, Chappuis-Flament S, Wong E, Gumbiner BM, Shapiro L. C-cadherin ectodomain structure and implications for cell adhesion mechanisms. *Science (80-)*. 2002; 296:1308–1313.
- Bosher SK, Warren RL. Very low calcium content of cochlear endolymph, an extracellular fluid. *Nature*. 1978; 273:377–378. [PubMed: 661948]
- Brasch J, Harrison OJ, Honig B, Shapiro L. Thinking outside the cell: how cadherins drive adhesion. *Trends Cell Biol*. 2012; 22:299–310. [PubMed: 22555008]
- Cailliez F, Lavery R. Cadherin mechanics and complexation: the importance of calcium binding. *Biophys J*. 2005; 89:3895–3903. [PubMed: 16183887]
- Cheung ELM, Corey DP. Ca^{2+} changes the force sensitivity of the hair-cell transduction channel. *Biophys J*. 2006; 90:124–139. [PubMed: 16214875]

- Courjean O, Chevreux G, Perret E, Morel A, Sanglier S, Potier N, Engel J, van Dorsselaer A, Feracci H. Modulation of E-cadherin monomer folding by cooperative binding of calcium ions. *Biochemistry*. 2008; 47:2339–2349. [PubMed: 18232713]
- Edgar RC. MUSCLE: multiple sequence alignment with high accuracy and high throughput. *Nucleic Acids Res*. 2004; 32:1792–1797. [PubMed: 15034147]
- Emsley P, Lohkamp B, Scott WG, Cowtan K. Features and development of Coot. *Acta Crystallogr D Biol Crystallogr*. 2010; 66:486–501. [PubMed: 20383002]
- Geng R, Sotomayor M, Kinder KJ, Gopal SR, Gerka-Stuyt J, Chen DHC, Hardisty-Hughes RE, Ball G, Parker A, Gaudet R, et al. Noddy, a mouse harboring a missense mutation in protocadherin-15, reveals the impact of disrupting a critical interaction site between tip-link cadherins in inner ear hair cells. *J Neurosci*. 2013; 33:4395–4404. [PubMed: 23467356]
- Gillespie PG, Muller U. Mechanotransduction by hair cells: models, molecules, and mechanisms. *Cell*. 2009; 139:33–44. [PubMed: 19804752]
- Grossman SR, Shlyakhter I, Karlsson EK, Byrne EH, Morales S, Frieden G, Hostetter E, Angelino E, Garber M, Zuk O, et al. A composite of multiple signals distinguishes causal variants in regions of positive selection. *Science (80-)*. 2010; 327:883–886.
- Grossman SR, Andersen KG, Shlyakhter I, Tabrizi S, Winnicki S, Yen A, Park DJ, Griesemer D, Karlsson EK, Wong SH, et al. Identifying recent adaptations in large-scale genomic data. *Cell*. 2013; 152:703–713. [PubMed: 23415221]
- Grubmuller H. Force probe molecular dynamics simulations. *Methods Mol Biol*. 2005; 305:493–515. [PubMed: 15943012]
- Harrison OJ, Brasch J, Lasso G, Katsamba PS, Ahlsen G, Honig B, Shapiro L. Structural basis of adhesive binding by desmocollins and desmogleins. *Proc Natl Acad Sci U S A*. 2016; 113:7160–7165. [PubMed: 27298358]
- Haussinger D, Ahrens T, Sass HJ, Pertz O, Engel J, Grzesiek S. Calcium-dependent homoassociation of E-cadherin by NMR spectroscopy: changes in mobility, conformation and mapping of contact regions. *J Mol Biol*. 2002; 324:823–839. [PubMed: 12460580]
- Hirano S, Takeichi M. Cadherins in brain morphogenesis and wiring. *Physiol Rev*. 2012; 92:597–634. [PubMed: 22535893]
- Howard J, Hudspeth AJ. Compliance of the hair bundle associated with gating of mechano-electrical transduction channels in the bullfrog's saccular hair cell. *Neuron*. 1988; 1:189–199. [PubMed: 2483095]
- Humphrey W, Dalke A, Schulten K. VMD: visual molecular dynamics. *J Mol Graph*. 1996; 14:27–28. 33–38.
- Indzhukulian AA, Stepanyan R, Nelina A, Spinelli KJ, Ahmed ZM, Belyantseva IA, Friedman TB, Barr-Gillespie PG, Frolenkov GI. Molecular Remodeling of Tip Links Underlies Mechanosensory Regeneration in Auditory Hair Cells. *PLoS Biol*. 2013; 11:e1001583. [PubMed: 23776407]
- Isralewitz B, Gao M, Schulten K. Steered molecular dynamics and mechanical functions of proteins. *Curr Opin Struct Biol*. 2001; 11:224–230. [PubMed: 11297932]
- Jaramillo F, Hudspeth AJ. Displacement-clamp measurement of the forces exerted by gating springs in the hair bundle. *Proc Natl Acad Sci U S A*. 1993; 90:1330–1334. [PubMed: 7679501]
- Jin X, Walker MA, Felsovalyi K, Vendome J, Bahna F, Mannepalli S, Cosmanescu F, Ahlsen G, Honig B, Shapiro L. Crystal structures of *Drosophila* N-cadherin ectodomain regions reveal a widely used class of Ca(2)+-free interdomain linkers. *Proc Natl Acad Sci U S A*. 2012; 109:E127–E134. [PubMed: 22171007]
- Jorgensen WL, Chandrasekhar J, Madura JD, Impey RW, Klein ML. Comparison of simple potential functions for simulating liquid water. *J Chem Phys*. 1983; 79:926–935.
- Kachar B, Parakkal M, Kurc M, Zhao Y, Gillespie PG. High-resolution structure of hair-cell tip links. *Proc Natl Acad Sci U S A*. 2000; 97:13336–13341. [PubMed: 11087873]
- Kazmierczak P, Sakaguchi H, Tokita J, Wilson-Kubalek EMM, Milligan RAA, Müller U, Kachar B, Muller U, Kachar B. Cadherin 23 and protocadherin 15 interact to form tip-link filaments in sensory hair cells. *Nature*. 2007; 449:87–91. [PubMed: 17805295]

- Lek M, Karczewski KJ, Minikel EV, Samocha KE, Banks E, Fennell T, O'Donnell-Luria AH, Ware JS, Hill AJ, Cummings BB, et al. Analysis of protein-coding genetic variation in 60,706 humans. *Nature*. 2016; 536:285–291. [PubMed: 27535533]
- Maeda R, Kindt KS, Mo W, Morgan CP, Erickson T, Zhao H, Clemens-Grisham R, Barr-Gillespie PG, Nicolson T. Tip-link protein protocadherin 15 interacts with transmembrane channel-like proteins TMC1 and TMC2. *Proc Natl Acad Sci U S A*. 2014; 111:12907–12912. [PubMed: 25114259]
- Manibog K, Li H, Rakshit S, Sivasankar S. Resolving the molecular mechanism of cadherin catch bond formation. *Nat Commun*. 2014; 5:3941. [PubMed: 24887573]
- Nagar B, Overduin M, Ikura M, Rini JM. Structural basis of calcium-induced E-cadherin rigidification and dimerization. *Nature*. 1996; 380:360–364. [PubMed: 8598933]
- Nakaya K, Harbidge DG, Wangemann P, Schultz BD, Green ED, Wall SM, Marcus DC. Lack of pendrin HCO₃⁻ transport elevates vestibular endolymphatic [Ca²⁺] by inhibition of acid-sensitive TRPV5 and TRPV6 channels. *Am J Physiol Renal Physiol*. 2007; 292:F1314–F1321. [PubMed: 17200157]
- Nicoludis JM, Lau SY, Scharfe CPI, Marks DS, Weihofen WA, Gaudet R. Structure and Sequence Analyses of Clustered Protocadherins Reveal Antiparallel Interactions that Mediate Homophilic Specificity. *Structure*. 2015; 23:2087–2098. [PubMed: 26481813]
- Oroz J, Valbuena A, Vera AM, Mendieta J, Gomez-Puertas P, Carrion-Vazquez M. Nanomechanics of the cadherin ectodomain: “canalization” by Ca²⁺ binding results in a new mechanical element. *J Biol Chem*. 2011; 286:9405–9418. [PubMed: 21177864]
- Otwinowski Z, Minor W. Processing of X-ray diffraction data. *Methods Enzym*. 1997; 276:307–326.
- Pepermans E, Petit C. The tip-link molecular complex of the auditory mechano-electrical transduction machinery. *Hear Res*. 2015; 330:10–17. [PubMed: 26049141]
- Phillips JC, Braun R, Wang W, Gumbart J, Tajkhorshid E, Villa E, Chipot C, Skeel RD, Kale L, Schulten K. Scalable molecular dynamics with NAMD. *J Comput Chem*. 2005; 26:1781–1802. [PubMed: 16222654]
- Pickles JO, Comis SD, Osborne MP. Cross-links between stereocilia in the guinea pig organ of Corti, and their possible relation to sensory transduction. *Hear Res*. 1984; 15:103–112. [PubMed: 6436216]
- Pokutta S, Herrenknecht K, Kemler R, Engel J. Conformational changes of the recombinant extracellular domain of E-cadherin upon calcium binding. *Eur J Biochem*. 1994; 223:1019–1026. [PubMed: 8055942]
- Saleha S, Ajmal M, Jamil M, Nasir M, Hameed A. In silico analysis of a disease-causing mutation in PCDH15 gene in a consanguineous Pakistani family with Usher phenotype. *Int J Ophthalmol*. 2016; 9:662–668. [PubMed: 27275418]
- Salt AN, Inamura N, Thalmann R, Vora A. Calcium gradients in inner ear endolymph. *Am J Otolaryngol*. 1989; 10:371–375. [PubMed: 2596623]
- Sawaya MR, Wojtowicz WM, Andre I, Qian B, Wu W, Baker D, Eisenberg D, Zipursky SL. A Double S Shape Provides the Structural Basis for the Extraordinary Binding Specificity of Dscam Isoforms. *Cell*. 2008; 134:1007–1018. [PubMed: 18805093]
- Siemens J, Lillo C, Dumont Ra, Reynolds A, Williams DS, Gillespie PG, Müller U. Cadherin 23 is a component of the tip link in hair-cell stereocilia. *Nature*. 2004; 428:950–955. [PubMed: 15057245]
- Söllner C, Rauch GJ, Siemens J, Geisler R, Schuster SC, the Tübingen 2000 Screen Consortium. Müller U, Nicolson T. Mutations in cadherin 23 affect tip links in zebrafish sensory hair cells. *Nature*. 2004; 428:955–959. [PubMed: 15057246]
- Sotomayor M, Schulten K. Single-Molecule Experiments in Vitro and in Silico. *Sci*. 2007; 316:1144–1148.
- Sotomayor M, Schulten K. The allosteric role of the Ca²⁺ switch in adhesion and elasticity of C-cadherin. *Biophys J*. 2008; 94:4621–4633. [PubMed: 18326636]
- Sotomayor M, Corey DP, Schulten K. In search of the hair-cell gating spring elastic properties of ankyrin and cadherin repeats. *Structure*. 2005; 13:669–682. [PubMed: 15837205]
- Sotomayor M, Weihofen WA, Gaudet R, Corey DP. Structural Determinants of Cadherin-23 Function in Hearing and Deafness. *Neuron*. 2010; 66:85–100. [PubMed: 20399731]

- Sotomayor M, Weihofen WA, Gaudet R, Corey DP. Structure of a force-conveying cadherin bond essential for inner-ear mechanotransduction. *Nature*. 2012; 492:128–132. [PubMed: 23135401]
- Tariq H, Bella J, Jowitt Ta, Holmes DF, Rouhi M, Nie Z, Baldock C, Garrod D, Taberero L. Cadherin flexibility provides a key difference between desmosomes and adherens junctions. *Proc Natl Acad Sci*. 2015:201420508.
- Tsukasaki Y, Miyazaki N, Matsumoto A, Nagae S, Yonemura S, Tanoue T, Iwasaki K, Takeichi M. Giant cadherins Fat and Dachsous self-bend to organize properly spaced intercellular junctions. *Proc Natl Acad Sci*. 2014; 111:16011–16016. [PubMed: 25355906]
- Vollrath MA, Kwan KY, Corey DP. The micromachinery of mechanotransduction in hair cells. *Annu Rev Neurosci*. 2007; 30:339–365. [PubMed: 17428178]
- Zhao Y, Yamoah EN, Gillespie PG. Regeneration of broken tip links and restoration of mechanical transduction in hair cells. *Proc Natl Acad Sci U S A*. 1996; 93:15469–15474. [PubMed: 8986835]

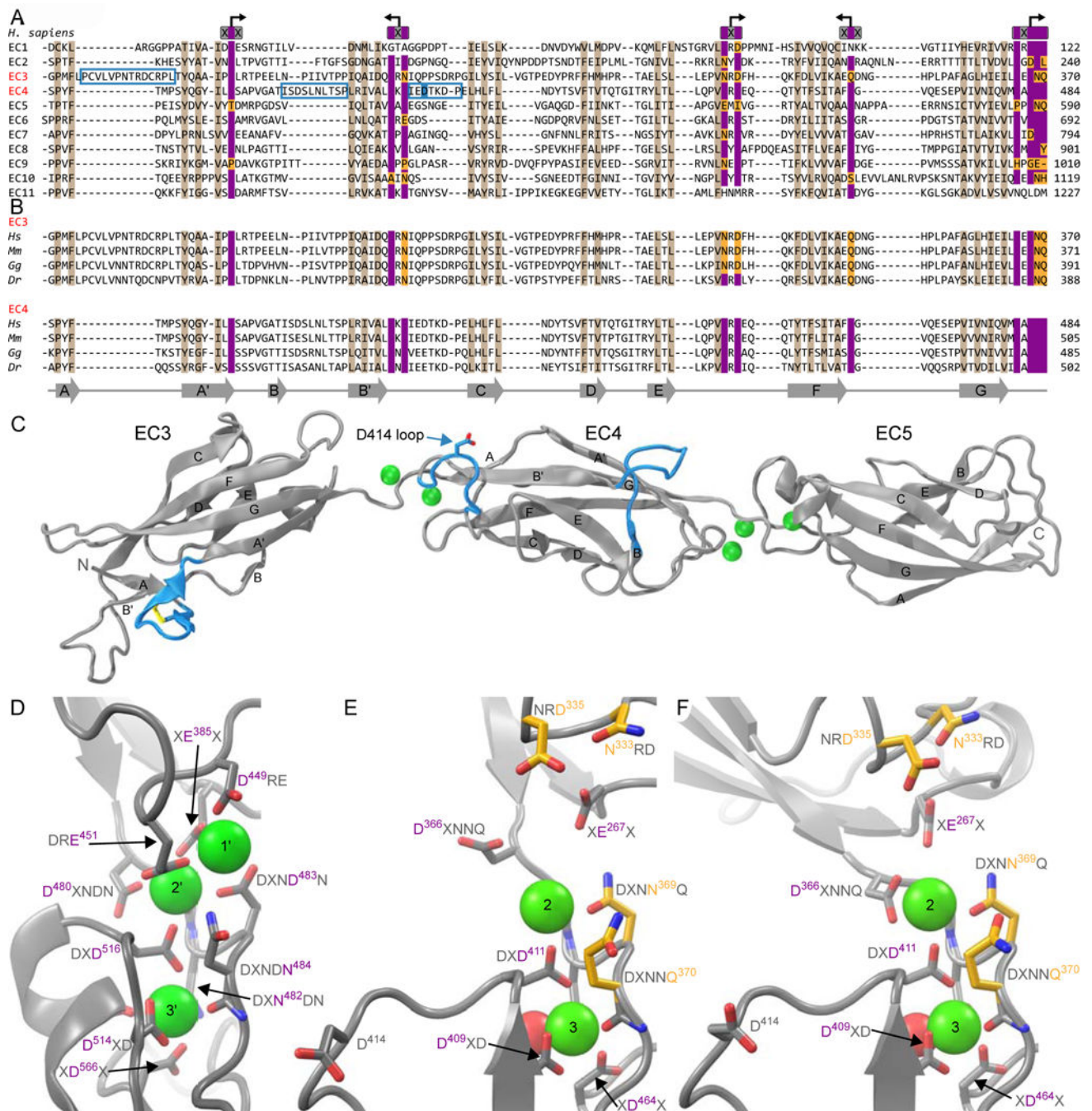


Figure 1. PCDH15 contains non-canonical linker regions including a novel partial Ca²⁺-free linker between EC3 and EC4

(A) Sequence alignment of *Homo sapiens* (*Hs*) PCDH15 EC repeats (NP_001136243.1). Ca²⁺-binding motifs are indicated at the top, with arrows pointing to the relevant preceding or proceeding linker region. Blue boxes mark loops discussed in main text. Highlights correspond to D414A polymorphism location (blue), hydrophobic core residues (brown), canonical Ca²⁺-binding motif residues (magenta), and departures from canonical Ca²⁺-binding sequences (orange). (B) Sequence alignments of EC3 and EC4 from various species (*Mm*, *Mus musculus*, NP_001142746.1; *Gg*, *Gallus gallus*, NP_001038119.1; *Dr*, *Danio*

rerio, NP_001012500.1). Secondary structure based on EC4 is indicated below. (C) Ribbon diagram of PCDH15 EC3-5. Green spheres are Ca^{2+} ions. Loops in blue are discussed in the text, and the D414 sidechain and cysteines forming a disulfide bond are shown as sticks. (D–F) Detail of linker regions and Ca^{2+} -binding sites for PCDH15 EC4-5 (D; chain A), EC3-4 (E; chain A), and EC3-4 (F; chain B). Ca^{2+} -binding motif residues are shown as sticks, with non-canonical substitutions in orange. A site 3 water molecule in EC3-4 is shown as a red sphere. See also Figures 2 and 3.

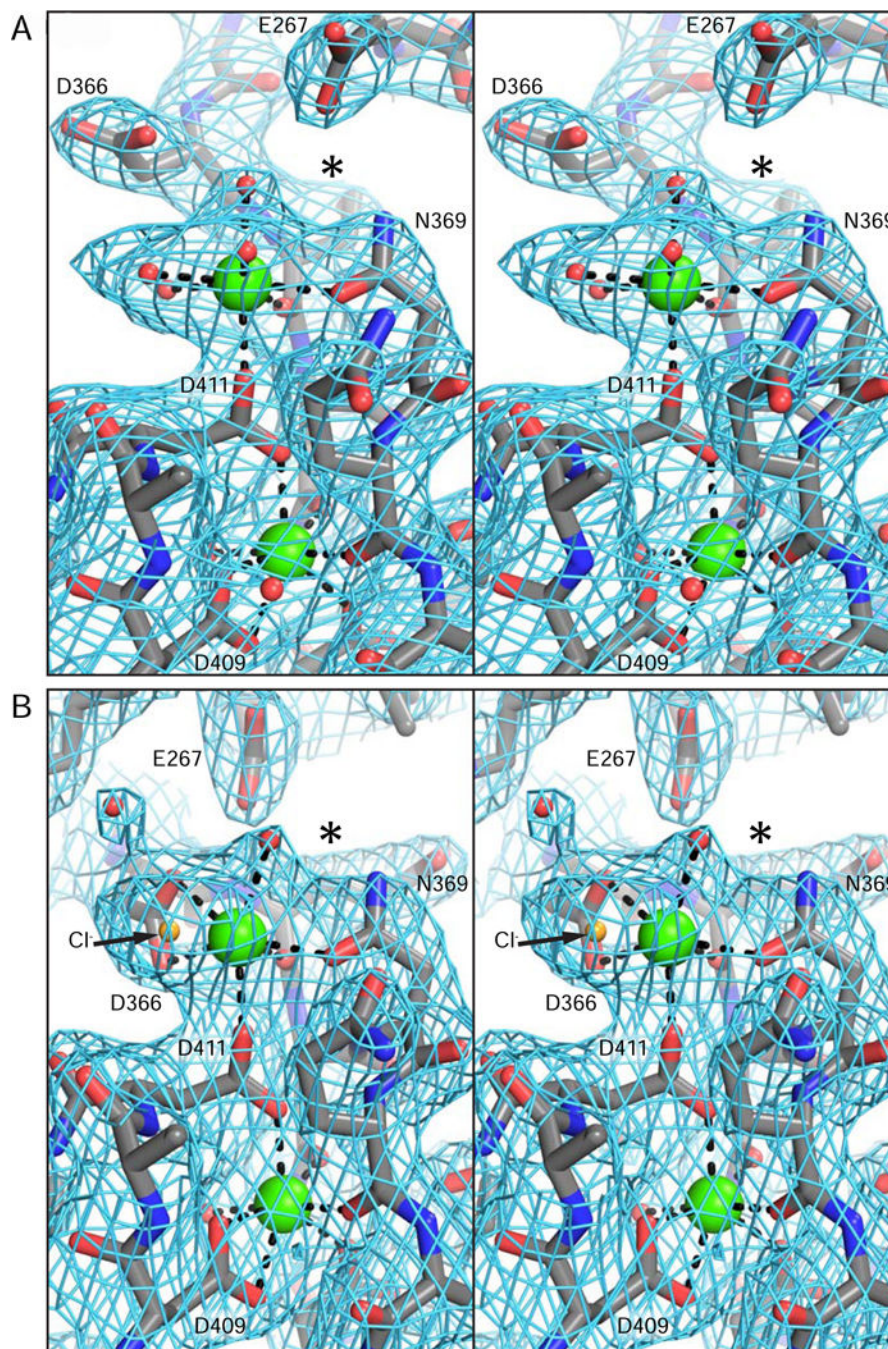


Figure 2. The EC3-4 linker region lacks electron density for a Ca²⁺ ion at site 1
Stereo representations of the weighted $2F_o - F_c$ electron density map of the EC3-4 linker region from the PCDH15 EC3-5 structure contoured at 1.2σ for (A) chain A and (B) chain B. The protein is depicted as grey sticks, Ca²⁺ ions as green spheres, a tentatively assigned Cl⁻ ion as an orange sphere, and water molecules as red spheres. The Cl⁻ ion was assigned based on a density larger than expected from a water molecule and the presence of Cl⁻ in the crystallization solution. Asterisk denotes a lack of density at Ca²⁺-binding site 1.

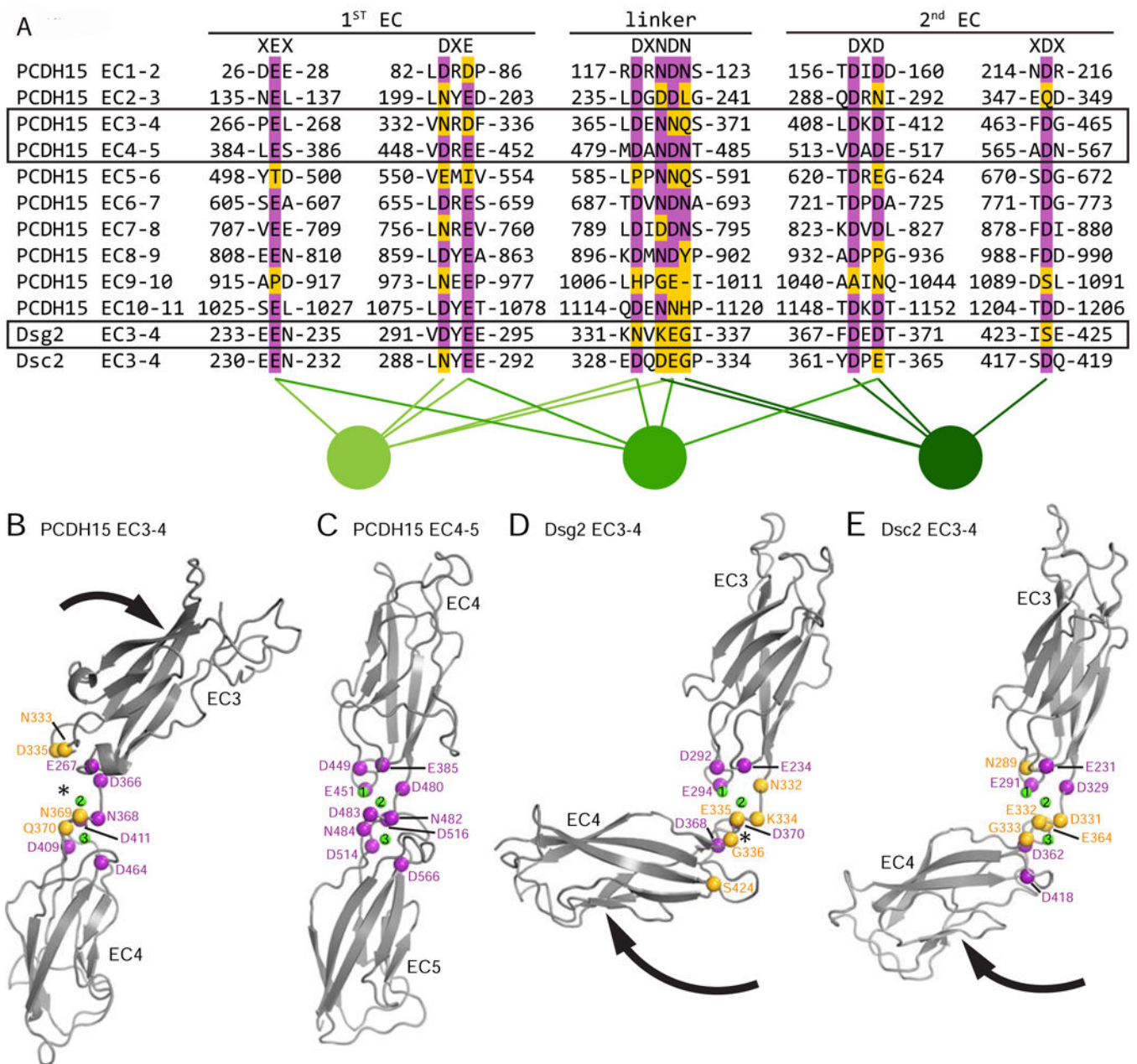


Figure 3. Partial Ca²⁺-free linkers alter inter-repeat connections

(A) Ca²⁺-binding motifs for each human PCDH15 (NP_001136243.1) linker aligned to the Desmoglein-2 (Dsg2; NP_001934.2) and Desmocollin-2 (Dsc2; AAH63291.1) EC3-4 linker motifs. Canonical and non-canonical residues are highlighted magenta and gold, respectively. Canonical Ca²⁺ coordination interactions are indicated at the bottom. (B–D) Cartoon representations of structures with partial Ca²⁺-free linkers (boxed in A): PCDH15 EC3-4 missing Ca²⁺ at site 1 (A); canonical linker PCDH15 EC4-5 (C); and Dsg2 EC3-4 missing Ca²⁺ at site 3 (D; PDB ID 5ERD). Spheres mark Ca²⁺ ions (green), and canonical (magenta) and non-canonical (gold) Ca²⁺-binding residue Ca positions. Asterisks indicate missing Ca²⁺ ion positions. Ca²⁺ ions are approximately aligned in the three panels to

emphasize how the absence of a Ca^{2+} correlates with displacement of the disconnected EC repeat. Displacement relative to the canonical PCDH15 EC4-5 structure is indicated with arrows. (E) Analogous representation of the Desmocollin-2 EC3-4 structure (PDB ID 5ERP), which despite coordinating three Ca^{2+} ions shows a bend similar to Desmogleins, likely due to the presence of multiple non-canonical Ca^{2+} -binding motifs.

Author Manuscript

Author Manuscript

Author Manuscript

Author Manuscript

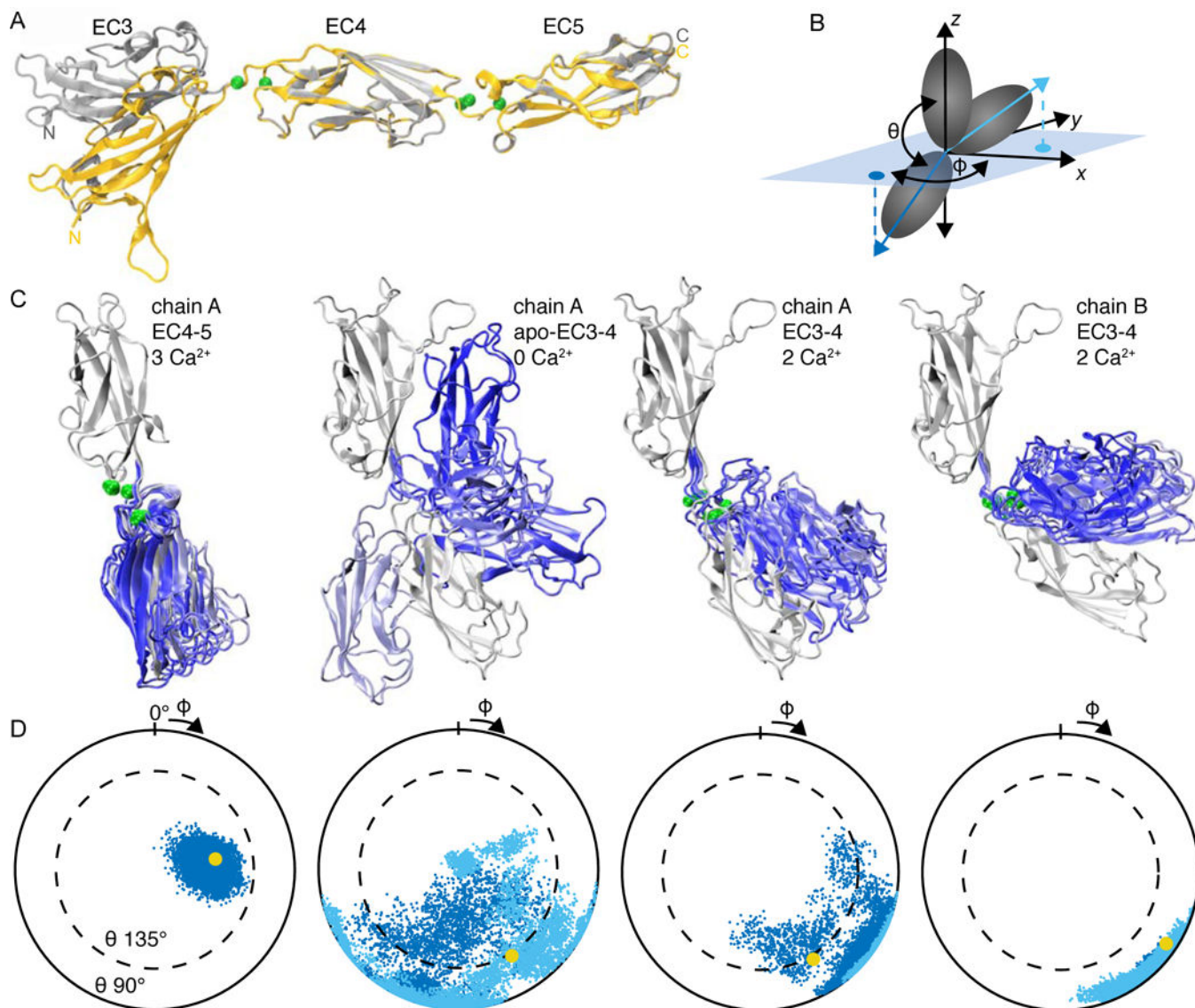


Figure 4. The EC3-4 partial Ca^{2+} -free linker of PCDH15 shows increased flexibility
 (A) Overlay of PCDH15 EC3-5 chains A (gray) and B (yellow). The orientation of EC3 with respect to EC4 is markedly different. (B) Inter-linker flexibility is quantified by aligning one repeat to the z -axis, computing the principal axes of the second repeat, and plotting the third principal axis projection in the x - y plane in a polar plot. Tilt (θ) and azimuthal angle (ϕ) are indicated. Projections of repeats below ($\theta > 90^\circ$) and above ($\theta < 90^\circ$) the x - y plane are dark and light blue, respectively. (C) Conformations at 20-ns intervals (grey to blue) throughout 100-ns equilibrium MD simulations were superimposed for two-repeat fragments with: a canonical linker (PCDH15 EC4-5 chain A; left; simulation S-1b); a Ca^{2+} -depleted linker (apo-EC3-4; middle left; S-2b); and two starting conformations of the partial Ca^{2+} -free linker, EC3-4 chain A (middle right; S-3b) and EC3-4 chain B (right; S-4b). Conformations were aligned using only the N-terminal EC repeat. For simplicity, only the initial N-terminal repeat conformation is depicted. (D) Inter-repeat linker flexibility during simulations computed as illustrated in (B). Panels are for PCDH15 fragments as indicated in (C). Initial

projection for each system is in yellow, with data plotted every 10 ps. See also Figures S1, S2, and S3.

Author Manuscript

Author Manuscript

Author Manuscript

Author Manuscript

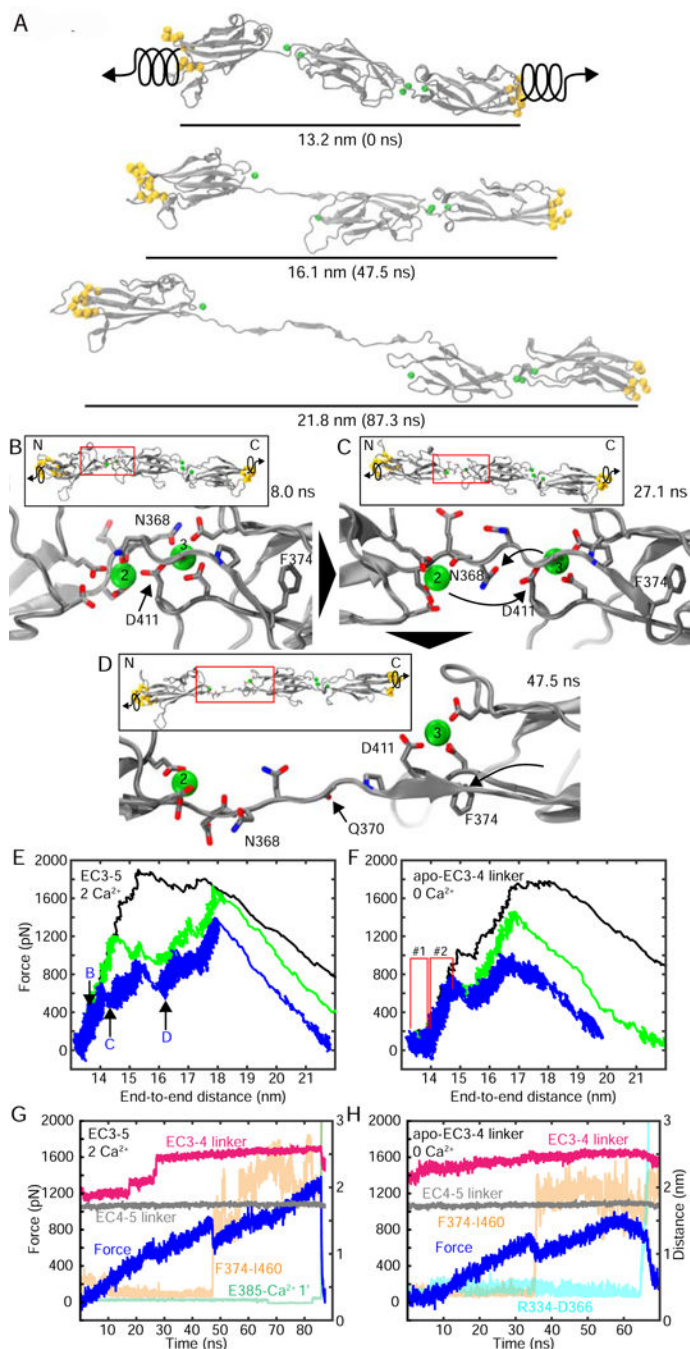


Figure 5. The EC3-4 partial Ca^{2+} -free linker unfolds before the EC4-5 canonical linker (A) Snapshots from SMD simulation S-7g depicting the initial conformation and mechanically induced unfolding states of EC3-5. Force was applied to the center of mass of atom groups (yellow spheres) at the N-($\text{Ca}^{242-244}$, 286, 287, 300, 301, 349–353) and C-($\text{Ca}^{498-500}$, 585–587, 553–555) termini. Springs indicate direction of applied force. The respective time points and center-of-mass distances are indicated below each snapshot. (B–D) EC3-4 linker conformations during simulation S-7g, depicting initial conformation (B) and specific rupture points (C–D). Curved arrows indicate displacement of residues of

interest from original positions. Entire EC3-5 fragment is shown in insets. (E) N-terminal applied force versus end-to-end distance for constant velocity stretching of EC3-5 (black: S-7e, 10 nm/ns; green: S-7f, 1 nm/ns; blue: S-7g, 0.1 nm/ns). Arrows indicate time points of snapshots in (B–D). (F) N-terminal applied force versus end-to-end distance for constant velocity stretching of EC3-5 where Ca^{2+} ions were removed from the EC3-4 linker (apo EC3-4 linker) (black: S-8e, 10 nm/ns; green: S-8-f, 1 nm/ns; blue: S-8g, 0.1 nm/ns). Two force-extension regimes with different elasticity are indicated by red lines. Data in (E–F) plotted every 4 ps. (G) Force applied to EC3-5 N-terminus (blue) and various measured distances versus time for simulation S-7g: EC3-4 linker length (L365 Ca to P372 Ca; magenta); EC4-5 linker length (M479 Ca to P485 Ca; grey); hydrophobic contact F374 C ζ to I460 C γ_2 (orange); and salt bridge E385 C δ to EC4-5 linker site 1' Ca^{2+} ion (cyan). (H) Same as (G) except for apo-EC3-4 linker (simulation S-8g), and salt-bridge distance between R334 C ζ and D366 C γ is depicted in cyan. Data in (G–H) plotted every 10 ps. See also Figures S4, S5, and S6.

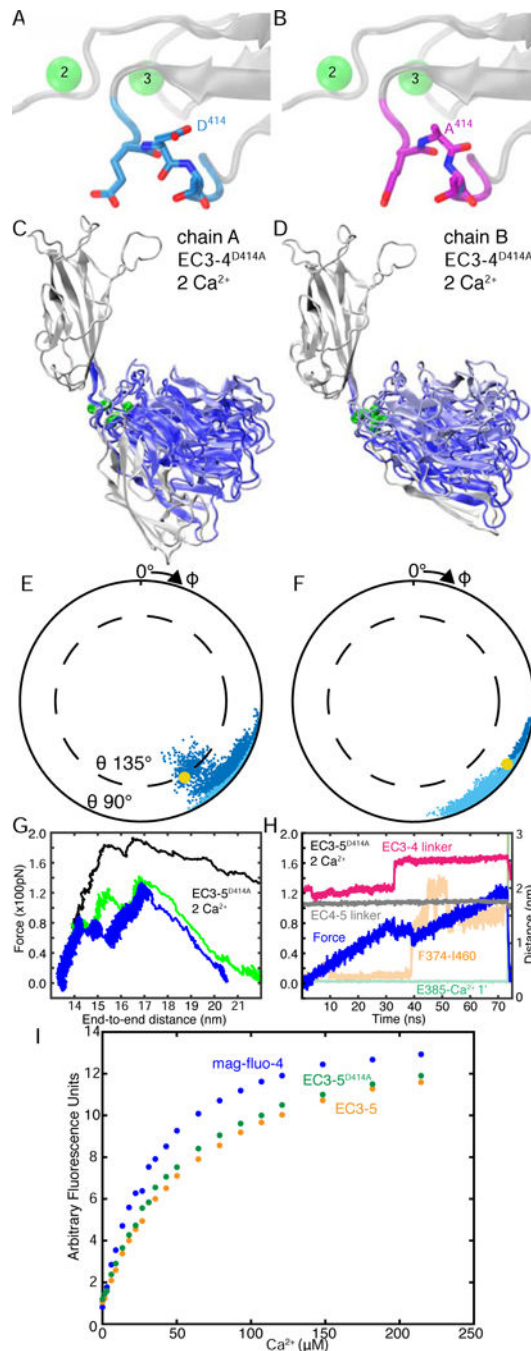


Figure 6. The D414A polymorphism does not impact PCDH15 structure, simulated dynamics, and predicted mechanical stability

(A and B) Detail of the D414 loop in structures of EC3-5 (A) and EC3-5^{D414A} (B). Residues E413-T415 are depicted as sticks, the rest of the protein as a gray cartoon, and sites 2 and 3 Ca²⁺ ions of the EC3-4 linker as green spheres. (C–D) Conformations at 25-ns intervals (gray to blue) from 100-ns equilibrium MD simulations for PCDH15 EC3-4^{D414A} chain A (C; S-5b) and chain B (D; S-6b) were superimposed using EC3 as reference. For simplicity, only the initial EC3 conformation is depicted. (E–F) Inter-repeat linker flexibility during simulations, computed as illustrated in Figure 4B, for EC3-4^{D414A} chain A (E) and chain B

(F). Initial projection for each system is yellow, and projections of repeats below ($\theta > 90^\circ$) and above ($\theta < 90^\circ$) the x - y plane are dark and light blue, respectively. Data in (E–F) plotted every 10 ps. (G) N-terminal applied force versus end-to-end distance for constant velocity stretching of EC3-5^{D414A} (black: S-9e, 10 nm/ns; green: S-9f, 1 nm/ns; blue: S-9g, 0.1 nm/ns). Data plotted every 4 ps. (H) Force applied to EC3-5^{D414A} N-terminus (blue, 0.1 nm/ns) and various measured distances versus time for simulation S-9g plotted every 10 ps for: EC3-4 linker length (L365 C α to P372 C α ; magenta); EC4-5 linker length (M479 C α to P485 C α ; grey); hydrophobic contact F374 C ζ to I460 C γ_2 (orange); and salt bridge E385 C δ to EC4-5 linker site 1' Ca²⁺ ion (cyan). (I) Fluorescence competition assay to measure the Ca²⁺ affinity of the EC3-4 linker. Mag-fluo-4 was titrated with Ca²⁺ as a control (blue curve). Competition between mag-fluo-4 and either EC3-4 (orange) or EC3-4^{D414A} (green) was used to determine approximate Ca²⁺ binding affinities of the two fragments. Representative curves of fluorescence versus Ca²⁺ are shown ($n = 4$). See also Figure S7.

Table 1

Data collection and refinement statistics.

	PCDH15 EC3-5	PCDH15 EC3-5 D414A	MmPcdh15 EC4-5
PDB ID	5T4M	5T4N	–
SBGridDB ID	361	363	362
Data collection			
Wavelength	0.98	0.98	0.98
Resolution range (Å) ^a	46.36–2.24 (2.32–2.24)	46.38–2.70 (2.80–2.70)	50.00–4.05 (4.12–4.05)
Space group	P 65	P 65	P 3 ₂ 21
Unit cell (a, b, c; Å)	105.61 105.61 193.67	105.66 105.66 193.77	144.30 144.30 73.14
Total reflections	168304 (13002)	235390 (22897)	13673 (670)
Unique reflections	57737 (5396)	33423 (3288)	7345 (356)
Multiplicity	2.9 (2.4)	7.0 (7.0)	4.3 (4.5)
Completeness (%)	98 (93)	99 (99)	99 (99)
Mean I/σ(I)	8.7 (0.7)	9.2 (0.6)	12.8 (3)
Resolution at I/σ(I) 1.5 (Å)	2.40	2.90	
Wilson B-factor	66.8	69.5	
R _{merge}	0.048 (1.41)	0.185 (3.50)	0.105 (0.524)
R _{meas}	0.059 (1.77)	0.199 (3.76)	
CC _{1/2}	0.997 (0.197)	0.996 (0.171)	
CC [*]	0.999 (0.573)	0.999 (0.54)	
Refinement			
Reflections used in refinement	57693 (3187)	33261 (3099)	
Reflections used for R-free	3626 (120)	2113 (126)	
R _{work}	0.189 (0.338)	0.203 (0.367)	
R _{free}	0.221 (0.319)	0.239 (0.386)	
CC _{work}	0.951 (0.385)	0.949 (0.330)	
CC _{free}	0.863 (0.338)	0.925 (0.299)	
Number of non-hydrogen atoms	5725	5627	
Macromolecules	5433	5354	
Ligands (Ca ²⁺ , Cl ⁻)	11 (10, 1)	11 (10, 1)	
Solvent	281	262	
Protein residues	693	684	
RMS(bonds)	0.011	0.012	
RMS(angles)	0.83	0.75	
Ramachandran favored (%)	97	98	
Ramachandran allowed (%)	2.9	2.2	
Ramachandran outliers (%)	0	0	
Rotamer outliers (%)	0	0	
Clashscore	0.84	1.32	

	PCDH15 EC3-5	PCDH15 EC3-5 D414A	MmPcdh15 EC4-5
Average B-factor	85.2	86.5	
Macromolecules	85.7	87.3	
Ligands	72.1	72.7	
Solvent	76.5	71.2	
Number of TLS groups	5	5	

^aStatistics for the highest-resolution shell are shown in parentheses.

Author Manuscript

Author Manuscript

Author Manuscript

Author Manuscript